SENSOR TASKING ANALYSIS FOR AN OPTICAL SENSOR NETWORK DESIGNED FOR COMPLETE GEO COVERAGE

Michael J. Rose[1] **and Carolin E. Frueh**[2]

[1]*Graduate Student, School of Aeronautics and Astronautics, Purdue University, United States of America, rose68@purdue.edu*

[2]*Associate Professor, School of Aeronautics and Astronautics, Purdue University, United States of America, cfrueh@purdue.edu*

ABSTRACT

Sensor networks that cover the whole geosynchronous object catalog in a single night are advantageous as they allow for full surveillance. In sensor tasking, often heuristic minimum local horizon elevation constraints are employed to avoid observation attempts that yield little return as the air-mass the reflected light from a space object passes through increases significantly with increasing zenith angle. Often when modelling the sensor's motion between one viewing direction and other, a constant repositioning time is used, which reduces the fidelity of the model. In this paper, heuristic elevation constraints are compared to using tasking based on rigorously defined probability of detection. The results are shown in a realistic 34 sensor setup using the Two Line Element catalog. Then, a variable repositioning time is derived from real world data, and the results of this modelled variable repositioning time are compared to a constant repositioning time.

1. INTRODUCTION

As the number of resident space objects (RSO) increases, the need to track and maintain a catalog of their states and uncertainties becomes essential for comprehensive Space Situational Awareness (SSA). With a majority of observations of RSOs coming from a limited number of ground-based sensors, this creates the need for an efficient and effective sensor tasking scheme [2, 7]. Sensor tasking is a well-investigated topic [10, 20, 21, 22, 23, 24, 25, 26, 27] to just name a few. Schildknecht [19] and Alfano [28] developed survey strategies based on the current catalog population without explicit information on particular space objects. Follow-up observations are based on a current catalog that requires being updated, as positional uncertainties grow over time. This can be formulated as an optimization problem: Hill et al. used a covariance-based optical sensor tasking approach [25], Sunberg et al. leveraged the advantages of an information-based sensor tasking [26]. Jaunzemis et al. used an evidence-based tasking scheme [22], Linares et al. [24] and Little et al. [10] investigated machine learning algorithms for solving the sensor tasking optimization. Frueh et al. [7] developed a scheme of sensor tasking fusing survey and follow-up in a single framework based on weighted viewing directions. Little et al. investigated classical and AI-based optimizers for the efficient solution [3]. Ackermann et al. optimizes the total number and location of ground-based sensors to view all GEO objects consistently every day, including local weather effects and light pollution at the sensor locations [11].

There are several limiting factors when using optical sensors to make observations. Of special interest in this paper is the comparison of heuristically imposed elevation constraints and the probability of detection of RSOs in a sensor network designed to provide complete coverage of the geosynchronous region in a single night. This work will assume the probability of detection model developed by Sanson and Frueh, and the signal-to-noise ratio (SNR) for CCD images developed by Merline and Howell, 1995 [8, 14, 16, 15, 18, 17]. Secondly, When considering the single and multi-sensor tasking problem, the time it takes for the sensor to move from one viewing direction to another, or the sensor's repositioning time (or slew time), changes depending on how far the repositioning distance is. Modeling this effect as a variable repositioning time however can be computationally more significant than just considering the repositioning time to be constant, though the model will more accurate. Because of the trade-off between computational time and simulation accuracy, choosing to model a variable repositioning time is not a trivial task [29, 2, 3, 30].

2. SENSOR TASKING AND LOCAL HORIZON LIMITATIONS

2.1. Sensor Tasking Algorithm

When analyzing the sensor tasking problem, an algorithm that chooses the viewing directions of each sensor must be used. This paper uses a modified version of the sen-

sor tasking algorithm presented in Frueh et al. in 2018, shown in Eq. (1) [3, 7].

$$\max A = \sum_{g=1}^{l} \sum_{f=1}^{m_g} \left(\sum_{i=1}^{n} \mu(\tilde{X}_i) \cdot P_d(h_{f,g}, \tilde{X}_i) \cdot \ d(h_{f,g}, \tilde{X}_i, P_i) \right) \tag{1}$$

A is the total number of RSOs to be observed. l is the total number of sensors observing in the time-frame, and m_g is the number of observations (or viewing directions) taken by each sensor g. n is the total number of RSOs to be observed in the time-frame. $\mu(\tilde{X}_i)$ is an object i specific value. This value can either be increased depending on facts like observability of object i [12], if object i has been observed or not (set as a 1 and 0 respectively), etc. In this paper, all objects are initially set with $\mu(\tilde{X}_i) = 1$ and then changed to 0 once the object has been observed. $P_d(h_{f,g}, \tilde{X}_i)$ is the probability of detection of object i. More detail on $P_d(h_{f,g}, \tilde{X}_i)$ is in Eq. (4). $d(h_{f,g}, \tilde{X}_i, P_i)$ is the probability that object i falls within the FOV grid choice centered at $h_{f,g}$. For this paper, two Scenarios are compared: the mean state of each object is considered, and covariance is ignored (i.e., the mean state of each object is the true state), and the covariance is considered [3, 7].

3. MINIMUM ELEVATION VERSUS PROBABILITY OF DETECTION

3.1. Minimum Elevation Constraint

This paper studies the outcomes of how a pre-defined minimum elevation constraint for a ground-based sensor affects its performance in the sensor tasking problem. To represent the RSOs in the optical sensor problem, a working frame must be chosen. Little and Frueh found that a representation of the RSO's states in hour angle and declination frame for optical sensors combines minimal linearization errors with computational advantages avoiding constant recomputation of the grid layout [9, 3]. A changing minimum elevation constraint (h_{min}) will affect the FOR of the sensor (and a higher elevation constraint will make the FOR smaller, respectively), and consequently the total number of possible viewing directions. A comparison of how a pre-defined h_{min} changes the total possible number of viewing directions is shown in Fig. 1.

The FOV for the grid-space created in Fig. 1 is 2.5° (which is used in the results section). The blue grids represent the viewing directions of a sensor with no elevation constraint ($h = 0°$), while the green grids represent the viewing directions a sensor with a 20° elevation constraint. The blue sensor system of $h = 0°$ has a total of 5073 possible viewing directions. On the other hand, when increasing the minimum elevation constraint to $h = 20°$, or the green sensor system, the total number of possible viewing directions decreases to 3634. If no other factors are included when observing the RSOs, it is expected that increasing the minimum elevation constraint decreases the number of RSOs seen per observation period.

3.2. Probability of Detection

The probability of detection formulated by Sanson and Frueh analyzes how noise values in the observation image affect the readability of the RSOs image [8]. To formulate this, the object's irradiance and signal function going into the optics of the sensor must be calculated:

$$I_{obj}(\bar{\lambda}) = I_{0,Sun} \frac{A}{\rho^2} \left(\frac{2C_d(\bar{\lambda})}{3\pi} (\sin\alpha + (\pi - \alpha)\cos\alpha) \right) \tag{2}$$

Here the irradiance $I_{obj}(\bar{\lambda})$ for spherical objects (also referred to as object brightness in this paper) is in units of watts per meter squared. $I_{0,Sun}$ is the irradiance of the sun, and A is the area of the object. This work is assuming all objects are spheres, so A remains constant. The true size and shape of the RSOs vary significantly. Operational satellites usually are attitude stabilized, thus the assumption of a sphere (constant area A) can be justified for the purpose of radiation effects. Debris objects usually do have significant attitude motion, allowing for an averaged shape-attitude profile. Albeit usually the attitude motion is not uniform, but as a first-order approximation the canon ball model can be justified [6]. Setting all objects to a constant spherical shape allows for easy computation of the irradiance of the objects, and general assumptions about the probability of detection can be made [3]. $C_d(\bar{\lambda})$ is the diffuse reflection parameter at an average wavelength (assumed to be 600 nanometers in this work), and α is the Sun-Object-Observer phase angle [4].

$$S_{sig,obj} \approx (D - d) \frac{\bar{\lambda}}{hc} exp(-\tau(\lambda) R(\zeta)) I_{obj}(\bar{\lambda}) L \tag{3}$$

This work assumes that the sensors are equipped with a charge-couple device (CCD) to capture the images. $S_{sig,obj}$ is the signal function of the irradiance passing through the optics. D is the primary radius of the sensor's optics, and d is the secondary radius. λ is the average wavelength of light reflected off and h and c are Boltzman's constant and the speed of light constant respectively (for the remaining of the paper, h will refer to the elevation in the sensor's azimuth, elevation frame). $\tau(\lambda)$ is the atmospheric extension coefficient, $I_{obj}(\bar{\lambda})$ is the irradiance described in Eq. (3) and L is the loss function for the specific sensor. $R(\zeta)$ is an atmospheric model used based on the zenith angle of the object. It is expected that as elevation increases, the probability of detection of an object increases on average as the light from the object has less attenuating air-mass to pass through [8, 4].

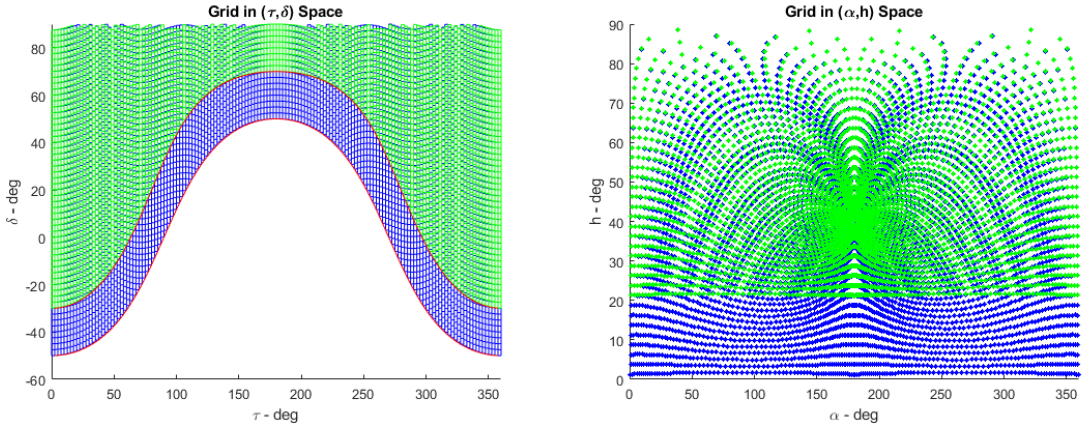

(a) τ, δ frame with no elevation constraint (blue) and 20° minimum elevation constraint (green)

(b) α, h frame with no minimum elevation constraint (blue) and 20° minimum elevation constraint (green)

Figure 1: Comparison of the effects of an elevation constraint on the sensor's FOR. There is a significant decrease in possible viewing directions in the working frame when comparing no elevation constraint system (blue) versus a 20° rigid elevation constraint system (green).

The atmospheric effects are taken into account by $R(\zeta)$. This leads to the following expression for the probability of detection [8]:

$$P_d = 1 - \frac{1}{2} \sum_{n=-\infty}^{n=\infty} \frac{\Gamma(n - \frac{g}{2}, \lambda_{obj,i} + \lambda_{S,i} + \lambda_{D,i})}{n!} \cdot \left(\text{erf}\left(\frac{n + 1 - t - \mu_{B,i}}{\sqrt{2g(\sigma_{B,i}^2 + \sigma_{R,i}^2)}} \right) - \text{erf}\left(\frac{n - t - \mu_{B,i}}{\sqrt{2g(\sigma_{B,i}^2 + \sigma_{R,i}^2)}} \right) \right) \tag{4}$$

Here t is the user-defined threshold SNR value set for each specific sensor based on its characteristics, $\mu_{B,i}$ and $\sigma_{B,i}^2$ are the mean and variance of the number of background pixels, $\sigma_{R,i}^2$ is the variance of the readout noise, and erf is the error function. In this work, t is defined as three standard deviations of the Merline noise [3, 8]. P_d has a range from zero to one, with an object having a $P_d = 0$ meaning there is a 0% probability of detecting that object, and a $P_d = 1$ meaning there is a 100% probability of detecting that object. The P_d is calculated for each object at each time. Then, a random number is chosen from a uniform probability distribution $C = U[0, 1]$. If $P_d \geq C$, then the object is considered detected at that time, otherwise it is not detected.

4. REPOSITIONING TIME OF OPTICAL SENSORS

When a sensor repositions to a new viewing direction to make an observation, it must slew in the azimuth direction and in the elevation direction. The time it takes for this sensor to slew, or reposition, to the new viewing direction is called the slew time or the repositioning time. The repositioning time in this work also considers the time it takes for the sensor to fully decelerate from repositioning, which is called the settling time. When designing a sensor tasking formulation, repositioning time needs to be considered. If repositioning time is considered constant, then the problem simplifies. However, a constant repositioning time may not be a valid assumption depending on how far the sensor has to reposition to its next viewing direction. If the sensor only needs to slew by one degree, then a constant repositioning time may be over accounting for this, and more observations can be made if the sensor tasking problem did not assume a constant repositioning time. If the sensor needs to slew 170° however, a constant repositioning time may under account for this, and the RSOs that the algorithm calculated to be in that viewing direction may not actually be there, causing errors in the model. This section will analyze the benefits and drawbacks of both assuming a constant repositioning time, as well as calculating and using a variable repositioning time.

4.1. Constant Repositioning Time

When using the sensor tasking optimization equation developed by Frueh et al. (2018), the time between observations, or the time between m_g and m_{g-1} needs to be defined [7]. This time can be different for each sensor depending on characteristics like the number of images taken, exposure time of those images, repositioning time, etc. The time between observations (t_{obs}) is given by the following [7, 3]:

$$t_{obs} = j \cdot t_{exposure} + (j - 1) \cdot t_{readout} + t_{repos} \tag{5}$$

where $t_{exposure}$ is the exposure time for each image j. $t_{readout}$ is the readout time of each image, and t_{repos} is

the time for the sensor to reposition to the specific viewing direction $h_{f,g}$ in the sensor's FOR. In this work, it is assumed that the readout time is smaller than the constant repositioning time, or $t_{repos} > t_{readout}$. This assumption allows for one of the images to be read while the sensor is repositioning, hence why in Eqn. (5) the readout time is multiplied by $(j-1)$ [7]. Eqn. (5) can be rewritten to separate the repositioning time from the image creation/processing time as follows:

$$t_{obs} = t_{img} + t_{repos} \tag{6}$$

where $t_{img} = j \cdot t_{exposure} + (j-1) \cdot t_{readout}$. Eqn. (6) is used regardless of if the repositioning time is constant or not, and for this work, it is assumed that t_{img} is constant, though can be different for each sensor.

If t_{repos} is set constant, then the simulation becomes computationally efficient. All the RSOs' states can be calculated beforehand at each m_g for each sensor, because of the constant repositioning time. However, if the repositioning time is not varying, then simulation errors can occur. This work assumes two cases when comparing the constant repositioning time:

1. **Case 1**: When the repositioning time is constant and is not being compared to the variable repositioning time, then the sensor tasking performance is the true performance in the simulation, but it creates a model mismatch when applied to an actual sensor.
2. **Case 2**: When the constant repositioning solution is directly compared to the variable repositioning time solution, which is the most realistic simulation to the actual sensor, the optimizer solution is analyzed further:
    a. **A**: If the constant assumed for the repositioning time is smaller than the actual variable repositioning time for that m_g, the sensor does not view the objects at the time. The optimizer knows this and will account for these "missed" objects in future viewing direction considerations.
    b. **B**: If the constant assumed for the repositioning time is smaller than the actual variable repositioning time for that m_g, the sensor does not view the objects at the time. The optimizer does not know this and assumes it detected the "missed" objects, even though they were never detected.

Case 1 will be used to analyze the results in Section 5.2, while Case 2 will be used to analyze the results in Section 5.3.

4.2. Variable Repositioning Time

The problem becomes significantly more complex if a constant repositioning time is not assumed. If the repositioning time is different for each viewing direction, then this increases the computational time of the simulation. Each RSO must now be propagated to the "pseudo" time. The "pseudo" time for each viewing direction is not the actual time that the observation is taken, but is the time the observation would be taken if the algorithm chooses this specific viewing direction. This is done for every single viewing direction because each viewing direction has its own repositioning time. To increase computational efficiency, RSOs that have a measurement uncertainty near the viewing direction being analyzed (a measurement standard deviation of 10) are propagated to that "pseudo" time instead of all RSOs for that specific viewing direction. Then, the viewing direction grid is chosen based on Eqn. 1, and the objects are actually propagated to the true chosen time for this specific viewing direction. This process is repeated until the observation period is completed. With the variable repositioning time, the simulation computational complexity now increases with the size of the FOV of that specific sensor: a smaller FOV equates to more viewing directions and therefore more "pseudo" times that need to be calculated, and therefore more propagation times for the RSOs.

4.2.1. Repositioning Equation Formulation

A function to calculate the repositioning time based on the change in viewing direction also needs to be defined. The time for the sensor to reposition from grid at time $(f-1)$ to grid at time (f), or $t_{repos}(h_{f,g})$ is given below:

$$t_{repos}(h_{f,g}) = \zeta \sqrt{\max(|\ \Delta\alpha\ |, |\ \Delta h\ |)} \tag{7}$$

Here, the change in azimuth and elevation ($\Delta\alpha$ and Δh respectively) is given as the form of $\Delta\alpha = \alpha_f - \alpha_{f-1}$ and $\Delta h = h_f - h_{f-1}$ in units of degrees. ζ is a constant that scales how long the repositioning time takes. It is assumed that as the sensor is repositioning in the azimuth direction it is also repositioning in the elevation direction at the same time, hence why only the maximum the combined viewing direction change is considered. This model is used to try to account for the ramp-up and ramp downtime of the sensors slew. Once the sensor has reached maximum velocity, it is assumed that the speed will remain constant until the sensor arrives close to the new viewing direction, then slow down. The actual real-world repositioning system will be more complex, but the model has been validated with the real repositioning times of the Purdue Optical Ground Station (POGS).

4.2.2. Optimizing for a Variable Repositioning Scenario

Rose (2020) analyzed several different repositioning models based off the real world repositioning time from POGS [1]. The most optimal repositioning model tested is Eqn. (7). From there, two scenarios will be tested in the variable repositioning analysis, shown in Section 5.3.

The first scenario will be using Eqn. (7), with $\zeta = 1$ (in this paper, only a comparison is shown with $\zeta = 1$, a full detailed analysis is shown in Rose (2020)) [1]. This scenario is used to try to understand the affects of a variable repositioning time when the t_{repos} is not significantly larger than t_{img}, from Eqn. (6). The other scenario will be using Eqn. (7), with $\zeta = 5$ to represent a sensor that has a slow repositioning rate.

The optimization strategy can easily be added into the formulation developed by Frueh et al. (2018). Modifying Eqn. (1) to consider the repositioning time weighting function $\gamma_{repo}(h_{f,g})$, the following is derived:

$$\max A = \sum_{g=1}^{l}\sum_{f=1}^{m_g}\left(\sum_{i=1}^{n}\left(\mu(\tilde{X}_i)\cdot P_d(h_{f,g},\tilde{X}_i)\cdot\ d(h_{f,g},\tilde{X}_i,P_i)\cdot\gamma_{repo}(h_{f,g})\right.\right. \tag{8}$$

Where $\gamma_{repo}(h_{f,g})$ is the repositioning time weight function for all viewing directions in the FOR for sensor g. $\gamma_{repo}(h_{f,g})$ can be defined as any function that considers the repositioning time of the sensor. The following equation is used in this work to define $\gamma_{repo}(h_{f,g})$:

$$\gamma_{repo}(h_{f,g}) = \begin{cases} 1 & 0 \le t_{repo}(h_{f,g}) < 1 \\ \dfrac{1}{C\cdot t_{repos}(h_{f,g})} + (1-\dfrac{1}{C}) & 1 \le t_{repo}(h_{f,g}) \end{cases} \tag{9}$$

$$C \ \ge \ 1 \tag{10}$$

$$\gamma_{repo}(h_{f,g}) = \begin{cases} 1 & 0 \le t_{repo}(h_{f,g}) < 1 \\ \dfrac{-t_{repos}(h_{f,g}) + max(t_{repos}(h_{f,g}))}{max(t_{repos}(h_{f,g})) - 1} & 1 \le t_{repo}(h_{f,g}) \end{cases} \tag{11}$$

$t_{repo}(h_{f,g})$ is calculated using Eqn. (7). Because an optimal $\gamma_{repo}(h_{f,g})$ function is unknown, several are tested in this work. C is a constant value that changes the penalty of the sensor choosing viewing directions that have a high repositioning time.

With a lower C value, the optimizer will prioritize repositioning times that are significantly shorter and viewing directions that are close to the current one. If the C value increases, the optimizer will still value shorter repositioning times over longer ones, but with less of an emphasis.

5. RESULTS

The sensor tasking optimization framework formulated by Frueh et al. (2018) is used to compare results from the single and multi-sensor tasking problems in this section [7]. A simple greedy algorithm developed by Little and Frueh (2019) is used to optimize the sensor tasking framework equation in this section [3]. Finally, the non-weighted and the additional variable repositioning weight factor on the sensor tasking optimization framework formulated by Frueh et al. (2018) and introduced in Section 4.2. The results of this section are split into two primary sections: A constant repositioning assumption and a variable repositioning framework.

5.1. Simulation Setup

For the object population of the RSOs, a two-line element (TLE) catalog of the night of March 19$^{\text{th}}$, 2019 was chosen for the initial states of the RSOs to try to minimize the differences in observation periods between different latitudes. This catalog was then reduced to analyze just GEO objects, assuming that GEO objects exist with a semimajor axis of $39,000\text{km} \le a \le 44,000\text{km}$ and an eccentricity of $e \le 0.5$. An Extended Kalman Filter is used for uncertainty propagation, and the covariance of each object is transformed into the working frame described in Fig. 1a. The initial mean state for the RSO is assumed to be the state given by the TLE set, and the initial covariance is defined for all RSOs as P_0, which is equal to $\sigma_x^2 = \sigma_y^2 = \sigma_z^2 = 50^2 km^2/s^2$, and $\sigma_{Vx}^2 = \sigma_{Vy}^2 = \sigma_{Vz}^2 = 1m^2/s^2$. As for the RSO specifics, though all RSOs have a variety of size, shape, and reflection properties, a constant set is defined for all of them, as precise information is mostly absent [3, 13]. All RSOs are modeled as spherical objects with a diameter of one meter, and a diffusion reflection parameter (C_d) of 0.26. The average wavelength of light reflecting off the RSO is assumed to be 600 nanometers, and the extinction coefficient is assumed to be 0.56. As for the Extended Kalman Filter, the process noise is assumed to be 1×10^{-6} and the measurement noise value is assumed to be one-arcsecond [3].

For the Ground-based Sensors, there are several constants that are assumed to be the same for all sensors. First, the FOV used in studying the multi-sensor setup from Ackermann et al. (2018) is assumed to be 2.5°. The readout time of the images is also assumed from the study to be zero seconds, the exposure time (or Δt from Eqn. 4) is set to 0.25 seconds, and the number of images taken for each observation time is 16 [11]. As for the optics, the primary radius is 0.3556 meters, the secondary radius is 0.165 me-

ters, and the camera gain is set to 1.4. The pixel scale in the CCD is 0.72 arcseconds per pixel, and the Quantum Efficiency is set to 0.6. As for the noise properties for calculating the SNR of an image, the readout noise is set to 10 and the dark noise is set to 5. The total number of background pixels per image is assumed to be 2000, and the intensity of light for the background is assumed to have a mean value of 1000 W/m^2 [3, 8]. These values correspond with Purdue Optical Ground Station (POGS). The constant repositioning time and heuristic minimum elevation constraint used in Section 5.2 will be presented as the results are shown, as they vary depending on the specific Scenario. The location for the multi-sensor Scenarios is taken from Ackermann et al. (2018). This multi-sensor system was developed to observe all GEO objects at least once each night. They vary between a latitude of $\pm$ 40°, vary in altitude, and span all longitudes [11].

5.2. P_d Versus Elevation Constraint in the Sensor Tasking Problem

To fully test the effects of elevation and the probability of detection of RSOs, the algorithm described in Eqn. (1) is used on a single sensor example. A simple greedy algorithm is used, which will be both computationally efficient and will get close to maximizing the total number of objects seen [3]. This analysis is split into two parts: First, the single and multi-sensor tasking problem will be analyzed assuming that the mean state of the object is the true state. Secondly, the same analysis is conducted and extended to include the uncertainty in the object's states using Eqn. (1).

5.2.1. Analysis Assuming The Mean State is the True State

The sensor/sensors will try to maximize the number of GEO objects seen at least once in the following three Scenarios:

1. Scenario 1: The RSOs will assume to have a $P_d = 1$ at all observation times
2. Scenario 2: The RSOs will have a variable P_d at all times, but the sensor tasking algorithm will not take this into account
3. Scenario 3: The RSOs will have a variable P_d at all times, and the sensor tasking algorithm will take this into account

First, the single sensor problem is studied. Each Scenario in Fig. 2 - 4 was run at eight different latitude values for the single sensor's location and nine different minimum elevation constraints.

Fig. 2 shows the first Scenario: The RSOs are assumed to have a $P_d = 1$ at all observation times. As the elevation

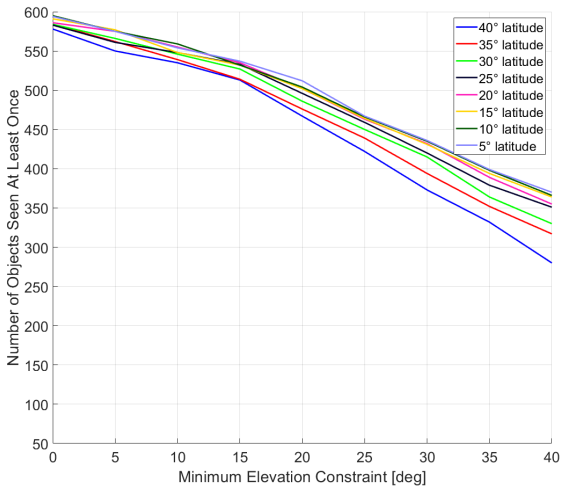

Figure 2: Scenario 1: The RSOs will assume to have a $P_d = 1$ at all observation times. This is the ideal case and does not represent the real world, but more of a "limit" on the total performance of the sensor.

constraint for all latitudes tested decreases, the total number of GEO objects seen at least once increases, which is expected. Because $P_d = 1$, there is no limiting factor on the detectability of the objects as elevation decreases. The only focus is the total possible viewing directions. As the minimum elevation constraint decreases, the total number of possible viewing directions increases.

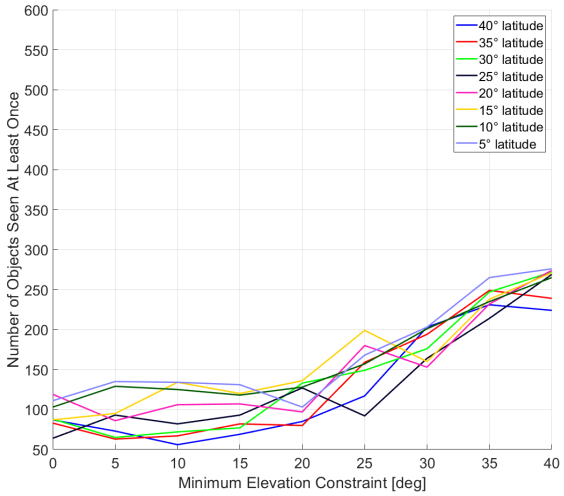

Figure 3: Scenario 2: The RSOs will have a variable P_d at all times, but the sensor tasking algorithm will not take this into account. This is the worst-case Scenario, and performance decreases significantly as the minimum elevation constraint decreases.

The second Scenario is shown in Fig. 3 and investigates the importance of taking into account the probability of detection in the sensor tasking optimization prob-

lem. Fig. 3 shows the results if the algorithm does not take into account the probability of detection of the objects when choosing an optimal viewing direction, but the total number of unique objects observed does take into account the probability of detection. For all latitudes tested, as the minimum elevation constraint decreases, the total number of unique RSOs also decreases. Because the algorithm is not taking into account the P_d of each object, once it has chosen all the viewing directions at higher elevations, it will choose the viewing directions at lower elevations, thinking that it is the optimal choice (because there are more objects now at those lower elevations with a $\mu(\tilde{X}_i) = 1$, which increases the weighting preference on that viewing direction). This implies, that a hard constraint on the minimum elevation (or a higher minimum elevation constraint) would improve the performance of the sensor's ability to see the most amount of objects if the sensor does not take into account the probability of detection.

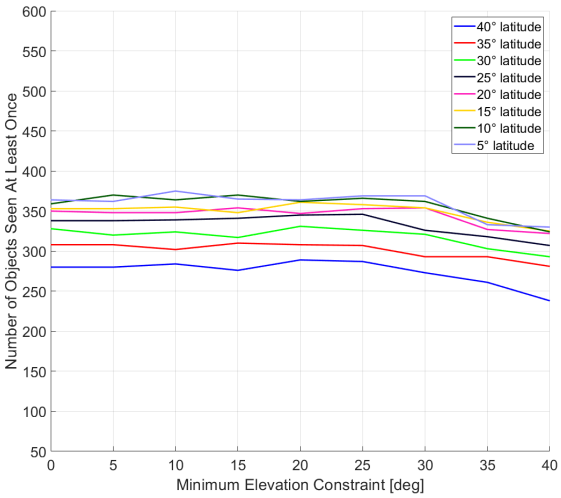

Figure 4: Scenario 3: The RSOs will have a variable P_d at all times, and the sensor tasking algorithm will take this into account. When the sensor is taking P_d into account, the performance increases as the minimum elevation constraint decreases, up to around 25° - 30° in this case.

For all latitude values tested in Fig. 4, it appears that once the minimum elevation constraint decreases to around 25° - 30°, the total number of unique objects seen stays relatively constant. This is due to the decreasing P_d values: for the entire solution space, once the elevation of the RSO decreased to a certain value (around 25° - 30° in this case), the probability of detection of that object becomes low. Because of the trend shown in Fig. 4, an elevation constraint is not useful when the sensor takes into account the probability of detection of the objects. The difference in performance at all latitudes and elevation constraints between Scenarios two and three shows that if the probability of detection of the objects is taken into account, the performance of the sensor increases without having to have a rigid minimum elevation constraint.

To fully determine the effects of the probability of detection on the sensor tasking problem, an analysis of more than one sensor needs to be done. The following will investigate the probability of detection on the multi-sensor tasking problem. The analysis will study the multi-sensor system set up by Ackermann et al. (2018) [11]. This section will be split up into the three Scenarios described above, and the same new two-line element catalog of the night of March 19^{th}, 2019 is used for each Scenario. More specifically, each of the three multi-sensor Scenarios will be run twice: one set will have all the sensors have a constant elevation constraint of 25°, and the other set will have no elevation constraint.

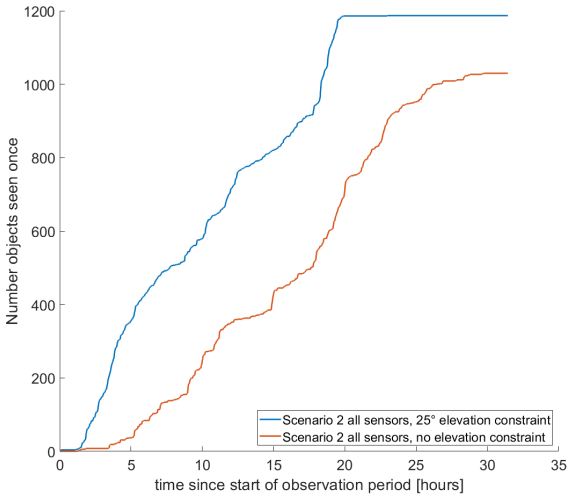

Figure 5: h_{min} Comparison for Scenario 2 in the Multi-Sensor System. When the P_d is not taken into account in the algorithm and there is no rigid elevation constraint, there is a significant loss in the multi-sensor tasking performance.

The results showed Fig. 5 are consistent with the conclusions made in the previous sections: when the probability of detection is not going to be considered in the sensor tasking algorithm, it is best to employ rigid elevation constraints on the sensors to achieve adequate results. The difference in performance between Scenario 2 with and without an elevation constraint shown in Fig. 5 is too much to ignore. Without a rigid elevation constraint in a sensor tasking algorithm that does not account for the probability of detection, the performance diminishes greatly.

When analyzing Fig. 6, the conclusions are consistent with the previous sections: when the probability of detection is taken into account into the sensor tasking algorithm, a rigid elevation constraint will not significantly change the performance, and in this case, actually decrease the performance, though very slightly. The only simulation difference between the red and blue lines of Scenario 3 is that the blue line has a rigid elevation constraint, and the red line does not. These results make sense because the rigid elevation constraint of 25° is

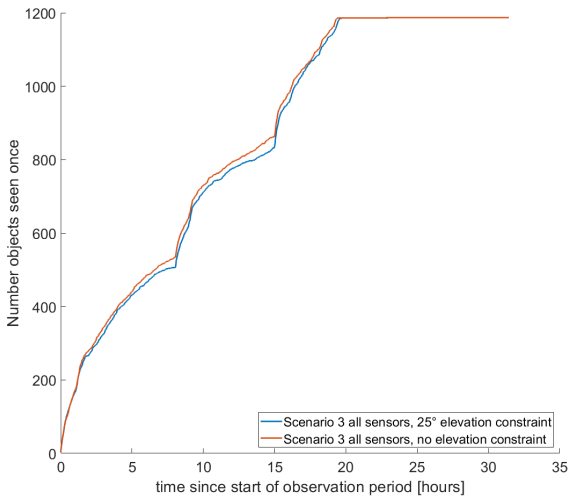

Figure 6: h_{min} Comparison for Scenario 3 in the Multi-Sensor System. When P_d is taken into account, there is no need to have a rigid elevation constraint on the sensors.

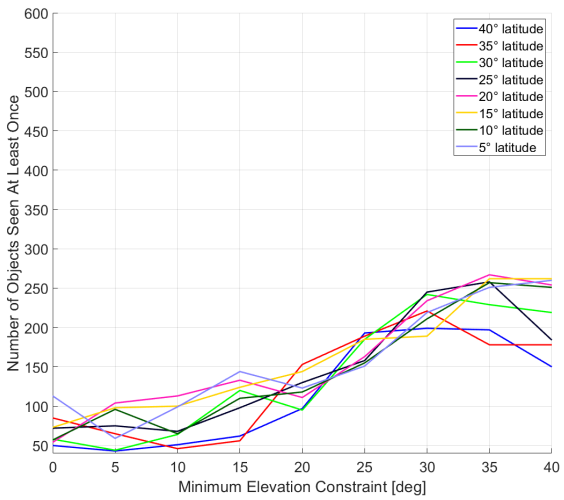

Figure 7: Scenario 2: The RSOs will have a variable P_d at all times, but the sensor tasking algorithm will not take this into account. Uncertainties in the RSOs' states are included in the analysis.

fairly strict. There is no significant computational difference between the multi-sensor system with the 25° elevation constraint on each sensor's FOR and the multi-sensor system with no elevation constraint. Overall, the following conclusions can be drawn: if the probability of detection is considered and modeled in the single and multi-sensor tasking problem, then a heuristic elevation constraint is not necessary. However, if the probability of detection is not considered, then a rigid elevation constraint of around 25° - 30° is recommended.

5.2.2. Analysis Considering Uncertainty in RSOs' States

The conclusions drawn from Section 5.2.1 assume that the mean state of the object retrieved from the Two-Line Element catalog is the actual state of the object. Now, the same analysis as before is done, but now uncertainties in the RSOs' states are considered. This increases the complexity of the problem, but also represents the real-world system with greater detail.

5.2.3. Single Sensor Analysis

In this section, only Scenario 2 and Scenario 3 described in Section 5.2.1 are shown, as Scenario 1 was used as a proof-of-concept for the simulation. Fig. 7 and 8 shows the results of Scenario 2 and Scenario 3 when uncertainty in the RSOs' states are considered.

Fig. 7 shows a similar trend as in Fig. 3. When P_d is not considered, the performance of the sensor decreases as the elevation constraint decreases. However, in Fig. 7, there appears to be a maximum in performance for this specific sensor Scenario when the rigid elevation constraint is set at around 25°-35° for all latitudes tested, with a majority of the latitudes tested having a maximum between 30°-35°. This may just be due to where the single sensor system is located and the specific TLE catalog used, but further testing has to be done, as well as how the uncertain states affect the multi-sensor tasking system.

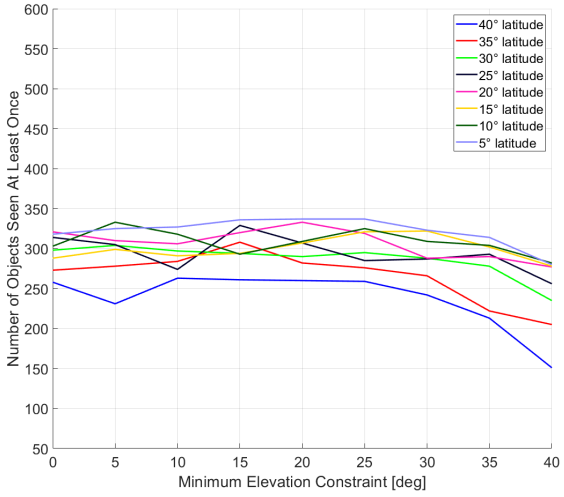

Figure 8: Scenario 3: The RSOs will have a variable P_d at all times, and the sensor tasking algorithm will take this into account. Uncertainties in the RSOs' states are included in the analysis.

Fig. 8 shows a similar trend as in Fig. 4. When P_d is considered, the performance of the single sensor increases as the rigid elevation constraint decreases until around an elevation constraint of 25°-30°, then performance increase

is minimal. The results when adding uncertain states to the RSOs is consistent with the results when the mean state is assumed to be the true state for the single sensor system.

5.2.4. Multi-Sensor Analysis

Now, the multi-sensor system is analyzed similar to Section 5.2.1, but now the calculation of the CDF at each observation is done. The same multi-sensor system developed by Ackermann et al. (2018) is implemented, and the same 1187 object set used in Section 5.2.1 for the night of March 19th, 2019 is studied. Scenario 2 and Scenario 3 are analyzed and compared side-by-side to each other, shown in Fig. 9 and Fig. 10.

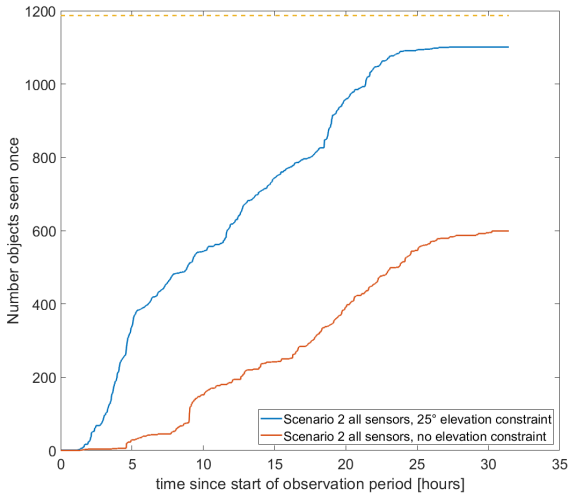

Figure 9: h_{min} Comparison for Scenario 2 in the Multi-Sensor System. Uncertainties in the RSOs' states are considered. There is a significant difference between the results due to P_d not being considered. The 34 sensor system does not observe all GEO objects when adding uncertainty in the RSOs' states. The dotted line is the total number of GEO objects to be observed (1187 in this example).

A few conclusions can be drawn from Fig. 9. The most relevant one is that when the uncertainty in the RSOs' states is considered, the multi-sensor system developed by Ackermann et al. (2018) does not observe all 1187 GEO objects for this night. This, however, is assuming P_d is not considered by the algorithm. For both cases ran for Scenario 2, with and without a rigid elevation constraint, the multi-sensor system was not able to detect all GEO objects, with 1101 objects detected when all sensors have a 25°, and only 599 objects detected when no rigid elevation constraint is employed, which is almost half as less as when the uncertainty is not considered, shown in Fig. 5.

Fig. 10 also shows that the multi-sensor system does not observe all GEO objects. 1112 objects are observed for

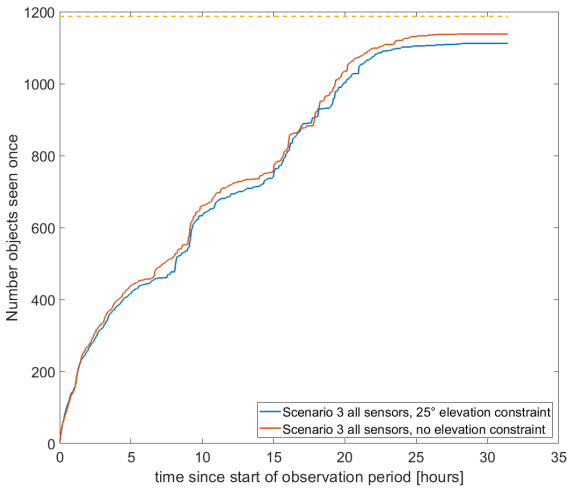

Figure 10: h_{min} Comparison for Scenario 3 in the Multi-Sensor System. When P_d is taken into account, there is no need to have a rigid elevation constraint on the sensors. The 34 sensor system does not observe all GEO objects when adding uncertainty in the RSOs' states. The dotted line is the total number of GEO objects to be observed (1187 in this example).

Scenario 3 when there is a 25° rigid elevation constraint on the sensors, while 1138 objects are observed when there is no rigid elevation constraint. The performance of Scenario 2 and Scenario 3 when there is a 25° elevation constraint is very similar, with only eleven total objects observed differences. This is consistent with Section 5.2.1 where the CDF was not calculated and simulated for the observation period. The difference between both of the Scenario 3 results is also consistent with that from Section 5.2.1, and as expected, the performance of the sensors with no rigid elevation constraint is slightly better than the performance with a rigid elevation constraint, though small.

When considering the uncertainty in the objects' states, the Ackermann et al. (2018) does not observe all cataloged GEO objects on the night of March 19th, 2019. Therefore, complete coverage of the GEO regime is not reached. As well, if a sensor system does not consider the probability of detection when choosing viewing directions, then a rigid elevation constraint of 25°-35° is recommended and has been shown to produce results close to the system that does model the probability of detection. If the probability of detection is modeled, however, then no rigid elevation constraint is needed if there are no natural obstructions near the sensor.

5.3. Variable Repositioning Analysis

This section will now look at the single sensor tasking problem, but now comparing the constant repositioning solution with the more real-world variable repositioning

model (case 2). The results in this section will be split up into two main focus areas: First, a comparison between several constant repositioning assumptions will be made with the true variable repositioning model. The performance will be compared for the two repositioning models of $\zeta = 1$ and $\zeta = 5$, where ζ is the constant multiplier from Eqn. (7) that determines how large of a factor the repositioning time is relative to the image processing time from Eqn. (6). Due to the limit of this paper, only the analysis, results and conclusions of $\zeta = 5$ will be shown, while just a comparison of the results from $\zeta = 1$ to $\zeta = 5$ will be presented. The analysis and results for $\zeta = 1$ can be found in Rose (2020) [1]. Then, the sensor tasking problem will consider various weight models on the variable repositioning time. These weight models will be compared to the unweighted variable repositioning time for both $\zeta = 1$ and $\zeta = 5$ repositioning models, where just a comparison with $\zeta = 1$ will be discussed.

5.3.1. Comparison of Constant and Variable Repositioning

In this section, the comparison of the assumed constant repositioning time to the real-world variable repositioning time will be made. For this section, three constant repositioning times will be analyzed: First, the "A to B" constant repositioning time will be modeled. This "A to B" repositioning time is calculated by finding the time it takes to reposition the sensor from any grid "A" to any other grid "B" using Eqn. (7). This is done for all viewing directions and is then averaged. This repositioning time will be less than the maximum possible repositioning time, which means that the system might not reach a specific viewing direction based on the assumed constant repositioning time. Therefore, Case 2A and Case 2B described in Section 4.1 will be studied to analyze the problem. The other two constant repositioning times that will be studied assume that the constant repositioning time is greater than or equal to the maximum possible repositioning time, and therefore no viewing direction can be missed when repositioning. More specifically, two constants will be studied, the constant repositioning time calculated be assuming that $\max(|\ \Delta\alpha\ |, |\ \Delta h\ |) = 180°$ at all times, or the maximum time assuming no unwinding is modeled, and $\max(|\ \Delta\alpha\ |, |\ \Delta h\ |) = 360°$ at all times, or assuming that this is the absolute maximum time with unwinding in the system. These two repositioning models will be referred to in this paper as "no unwind max" and "unwind max", described in Tab. 1.

Table 1: Maximum Constant Repositioning Time Models. The formulation is derived from Eqn. 7.

Constant Repositioning Time Model	Repositioning Time Calculations
no unwind max	$\max(\|\ \Delta\alpha\ \|, \|\ \Delta h\ \|) = 180°$
unwind max	$\max(\|\ \Delta\alpha\ \|, \|\ \Delta h\ \|) = 360°$

All these repositioning times will be studied for the test Scenarios of $\zeta = 5$ described in Eqn. 7 and Section 4. The single sensor that is is located at a latitude of 19.29° and a longitude of 166.61°, for the night of March 19th, 2019 [11].

5.3.2. Sensor with Constant Repositioning Multiplier $\zeta = 5$

The constant repositioning times used for this section with Constant Repositioning Multiplier $\zeta = 5$ is shown in Tab. 2.

Table 2: Constant Repositioning Time Models for constant repositioning multiplier $\zeta = 5$. These times are calculated based on Eqn. (7).

Constant Repositioning Time Model	Repositioning Time [sec]
A to B	42.98
no unwind max	67.08
unwind max	94.87

In this Scenario, the "A to B" constant repositioning time is calculated to be around 42.98 seconds, with the maximum calculated repositioning time being around 67.08 seconds. This allows for the comparison of a Scenario where t_{repos} is significantly larger than t_{img} from Eqn. (6), where $t_{img} = 4$ seconds. The $\zeta = 5$ model is also the model that closely models the POGS sensor.

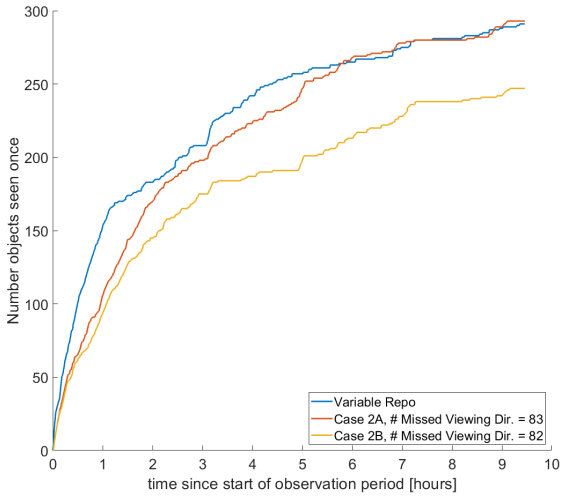

Figure 11: "A to B" Constant Repositioning Time, $\zeta = 5$. This Constant Repositioning time is equal to about 42.98 seconds, for this sensor system.

Fig. 11 shows the results when Case 2A and Case 2B apply to an assumed constant repositioning time for $\zeta = 5$. For Case 2A and Case 2B, the total number of observations for the night was 726. Several conclusions can be drawn from Fig. 11: if the sensor knows that it "missed"

a viewing direction and takes it into account, then the performance is close to the performance of the actual, variable repositioning model. However, if the algorithm does not take the missed viewing directions into account, then the performance of the sensor decreases. In Case 2A, the total number of viewing directions missed is a larger percentage of the total of observations made, but the system still has plenty of other opportunities to observe the objects it did miss. From Rose (2020), $\zeta = 1$ has similar results as $\zeta = 5$ [1].

Now, the "no unwind max" and the "unwind max" models will be compared with the true, variable repositioning model. The assumed repositioning time for these models is around 67.08 seconds and 94.87 seconds respectively. The results are shown in Fig. 12.

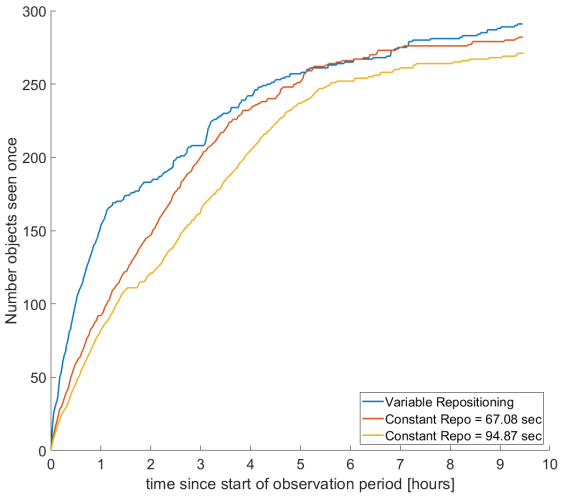

Figure 12: Comparison of the maximum and the unwinding maximum repositioning time (calculated from Eqn. (7)) for $\zeta = 5$. It is assumed that the maximum slew distance is 180°, and twice the unwinding maximum is a slew distance of 360°.

Fig. 12 shows that the performance of the assumed constant repositioning models are similar to the true, variable repositioning model. The total number of observations made for the constant repositioning models were 480 and 346 for the "no unwind max" and the "unwind max" models respectively. However, in Fig. 12, both the "no unwind max" and the "unwind max" models perform worse than the variable repositioning model. When $\zeta = 5$, the repositioning time is generally greater and therefore is a larger factor in the sensor tasking problem. Therefore, it is expected that if the repositioning time becomes a greater factor, then the variable repositioning model will generally produce a more optimal result than the assumed repositioning times that are greater than the maximum calculated repositioning times. These results were not shown for the $\zeta = 1$ case, as the repositioning time was not a significant factor in the sensor tasking [1].

For $\zeta = 5$, if the constant repositioning time is less than the maximum repositioning time, then like for $\zeta = 1$, if the algorithm does not consider when its constant repositioning is less than the actual repositioning for an observation, then there is a decrease in performance. If the algorithm does account for this, then the performance is similar to that of the true, variable repositioning time. For an assumed constant repositioning time that is greater than the maximum, there is a small difference in solutions between $\zeta = 1$ and $\zeta = 5$. If $\zeta = 5$, then the assumed constant repositioning times that are larger than the maximum calculated repositioning times perform worse than if $\zeta = 1$ [1].

5.3.3. Optimizing with Repositioning Time Considerations

Now, the optimizers described in Section 4.2.2 and Eqn. (8) using the single sensor system will be analyzed to study the benefits and drawbacks of considering the variable repositioning time in the sensor tasking framework. As in Section 5.3.1, the repositioning calculations using $\zeta = 1$ and $\zeta = 5$ will be tested. From here, four weighted repositioning time optimizers will be analyzed and compared to the unweighted variable repositioning time. These optimizers use the constant value described in Eqn. (9) that change the amount of weight given to the repositioning time, and are described as "C". The constant Cs that are used are C = 1, C = 2.5, C = 5. The linear weighted repositioning model described in Eqn. (11) is also analyzed alongside the C values.

5.3.4. Sensor with Constant Repositioning Multiplier $\zeta = 5$

The sensor with the repositioning calculation of $\zeta = 5$ is analyzed. This model increases the overall repositioning time between viewing directions, so it is expected that there will be some differences between these weighted models and the weighted models described for $\zeta = 1$ in Rose (2020) [1].

Because the repositioning time is greater in Fig. 13, it is expected that the total number of viewing directions should decrease from the $\zeta = 1$ case shown in Rose (2020) [1]. For the unweighted solution, a total of 6220 observations, while C = 1, C = 2.5, C = 5, and the linear model had a total of 8444, 7239, 6866, and 7628 observations for the night respectively. The total number of observations is also displayed in Tab. 3.

The total number of observations is indeed less, but not significantly, and hence why in Fig. 13 the optimizers do not perform significantly better than the unweighted solution. C = 1 is also significantly less than all other optimizers. This is due to the weight on the repositioning time being too heavy. In fact, in the model where the repositioning time from one viewing direction to another is larger ($\zeta = 5$), C = 1 performs worse than the same weight model in the Scenario where the repositioning time is smaller from one viewing direction to another

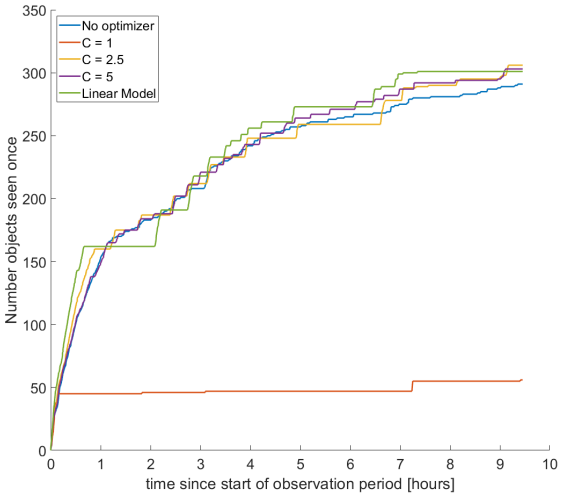

Figure 13: Comparison of Repositioning Weight Functions for $\zeta = 5$. For this example, the weight models described in Section 4 do have performance increase above the unweighted solution, besides the constant weight value C = 1 model described in Eqn. (9).

Table 3: Total number of observations for weighted repositioning models for constant repositioning multiplier $\zeta = 5$.

Weighted Repositioning Model	Total Number of Observations
Unweighted Model	6220
C = 1	8444
C = 2.5	7239
C = 5	6866
Linear Model	7628

($\zeta = 1$, in Rose (2020)) [1]. In Fig. 13 however, all the weighted optimizers besides C = 1 do perform better than the unweighted solution. This suggests that the model can be optimized when repositioning time is considered and if the repositioning time is large enough to play an important factor. However, the weighted models that do outperform the unweighted model do not outperform significantly. This suggests that, as stated in the previous sections, the variable repositioning factor is not too significant of a factor to consider in the sensor tasking formulation. This will have to be studied further for sensors where the t_{img} is a larger factor in the observation process, as described in Eqn. (6). In this analysis, t_{img} was small and therefore allowed for a large number of observations to be made. If t_{img} was larger, fewer observations would have been made, and therefore the time saved from choosing viewing directions that result in a low repositioning time would have been a greater factor in the sensor tasking problem.

6. SUMMARY

This paper analyzed the sensor tasking optimization for a single electro-optical sensor and a multi electro-optical sensor network for complete coverage of the geosynchronous region. The goal of this paper is to understand the optical and physical assumptions on a ground-based sensor, and how these assumptions affect the single and multi-sensor tasking problem. First, what is the effect of the probability of detection on the sensor tasking, especially when compared to rigid elevation constraints? Secondly, can the framework from Frueh et al. (2018) be expanded towards complete coverage of the GEO regime [3, 7]? Are the assumptions of Ackermann et al. (2018) correct [11]? Finally, how much of a benefit is there to modeling the computationally expensive variable repositioning time in the sensor tasking framework to achieve more accurate simulation models? If incorporated, can an optimizing strategy be developed to improve the performance of the sensor tasking problem?

6.1. Conclusions

In this paper a sensor tasking framework for complete coverage of the geostationary (GEO) objects has been introduced. The focus of the investigation was laid on two specific aspects. First: Is it advantageous to have a rigid heuristic minimum elevation constraint or should rather be a probability of detection model be employed. Secondly: Should the exact repositioning time of the sensor be taking into account, at a significant computational cost or are average repositioning times sufficient? In both aspects the target function is to reach a complete coverage of the entire GEO region within 24 hours.

In this paper it has been shown that a computation of the probability of detection is advantageous in all cases and makes a minimum elevation constraint obsolete. For the case where the probability of detection was not calculated, the maximum performance of the single sensor was achieved with an elevation constraint between 25° - 35°, and beyond that, the performance decreased significantly. Performance is worst, when neither, elevation constraint nor probability of detection is used.

For the variable repositioning time, several models have been developed and cases were studied. In the cases that were investigated, when the constant non-exact repositioning time used in the sensor tasking optimization is less than the true maximum repositioning time of the sensor, there can occur a significant decrease in performance. Performance for the complete GEO coverage case is not significantly impacted by a constant non-exact repositioning time in the sensor tasking optimizer, when this time is larger than the actually longest true repositioning time of the sensor.

In terms of full GEO coverage, using a system of 34 ground-based distributed optical sensors with a field of view of 2.5° elevation constraint as proposed Ackermann

et al., no full coverage of all known GEO objects can be reached when non-negligible uncertainty in the object's states is assumed, even when including exact probability of collision computation. Full coverage could be reached when object states were assumed to be exactly known.

7. ACKNOWLEDGMENT

We would like to acknowledge the support of this work via the Air Force Grant: AF16-AT05. We would like to thank and acknowledge the collaboration with Dr. Peter Zimmer and Dr. Mark Ackermann at J.T. McGraw and Associates. Special thanks go to Dr. Bryan Little AFIT Ohio, who we owe much in this paper from his previous work.

REFERENCES

[1] Rose, Michael James (2020): Optical Sensor Uncertainties and Variable Repositioning Times in the Single and Multi-Sensor Tasking Problem. Purdue University Graduate School. Thesis. https://doi.org/10.25394/PGS.13356188.v1

[2] David A. Vallado. *Fundamentals of Astrodynamics and Applications*, 3rd ed., Microcosm Press/Springer, 2007.

[3] Bryan Little. *Optical Sensor Tasking Optimization For Space Situational Awareness*, Ph.D, Purdue University, 2019.

[4] Carolin Frueh. *section 4. Observations*, AAE 590: Space Traffic Management, Lecture Script, Purdue, School of Aeronautics and Astronautics, 2019

[5] Carolin Frueh. *section 5. Coordinate Systems and Time*, AAE 590: Space Traffic Management, Lecture Script, Purdue, School of Aeronautics and Astronautics, 2019

[6] Roshan Thomas Eapen and Carolin Frueh. *Averaged Solar Radiation Pressure Modeling for High Area-to-Mass Ratio Objects in Geosynchronous Orbits*, Advances in Space Research, Vol. 63, Issue 1, pp. 127-141, doi:10.1016/j.asr.2018.03.042, 2018

[7] Frueh, C., Fiedler, H., and Herzog, J., "Heuristic and Optimized Sensor Tasking Observation Strategies with Exemplification for Geosynchronous Objects," *Journal of Guidance, Control, and Dynamics*, Vol. 41, No. 5, 2018, pp. 1036–1048. doi: 10.2514/1.G003123.

[8] F. Sanson, C. Frueh, "Noise Estimation and Probability of Detection in non-resolved Images: Application to Space Object Observation", *Advances in Space Research*, submitted 2018

[9] P.C. Mahalanobis. "On The Generalized Distance in Statistics". In *National Institute of Science*, volume 2, pages 49-55, India, 1936

[10] Little, B. D., and Frueh, C., "SSA Sensor Tasking : Comparison of Machine Learning with Classical Optimization Methods," *Advanced Maui Optical and Space Surveillance Technologies Conference*, 2018, pp. 1–17.

[11] Ackermann, M., Kiziah, R., Zimmer, P., and J.T. McGraw and Associates, "Weather Considerations for Ground-Based Optical Space Situational Awareness Site Selection", *Advanced Maui Optical and Space Surveillance Technologies Conference*, 2018.

[12] Friedman, A. M., and Frueh, C., "Determining characteristics of artificial near-Earth objects using observability analysis," *Acta Astronautica*, Vol. 144, 2018, pp. 405–421. doi:10.1016/j.actaastro.2017.12.028, URL https://linkinghub.elsevier.com/retrieve/pii/S0094576517307737.

[13] C. Früh, M. Jah, "Efficient High Area-to-Mass ratio (HAMR) Object Propagation including Self-Shadowing," Acta Astronautica, Vol. 95, pp. 227 - 241, 2014

[14] J. R. Janesick, T. Elliott, S. Collins, M. M. Blouke, J. Freeman, "Scientific Charge-Coupled Devices," Opt. Eng. 26(8) 268692 (1 August 1987) https://doi.org/10.1117/12.7974139

[15] Sanson, F., and Frueh, C., "Quantifying uncertainties in signal position in non-resolved object images: Application to space object observation", *Advances in Space Research*, Vol. 63, No. 8, 2019, pp. 2436-2454. https://doi.org/10.1016/j.asr.2018.12.040

[16] Hagen, N., and Dereniak, E., "Gaussian profile estimation in two dimensions", Applied Optics, Vol. 47, No. 36, 2008, p. 6842. https://doi.org/10.1364/AO.47.006842

[17] Houtz, N., Frueh, C., 2018. "Streak detection and characterization in ground-based optical observations of space objects". AAS/AIAA Astrodynamics Specialist Conference, Snowbird, Utah, August.

[18] Merline, W., and Howell, S., "A realistic model for point-sources imaged on array detectors: The model and initial results", Experimental Astronomy, Vol. 6, No. 1-2, 1995, pp. 163-210. https://doi.org/10.1007/BF00421131

[19] Schildknecht, T., Hugentobler, U., and Ploner, M., "Optical surveys of space debris in Geosynchronous Earth Orbit", *Advances in Space Research*, Vol. 23, No. 1, 1999, pp. 45-54. https://doi.org/10.1016/S0273-1177(98)00229-4

[20] R. Linares and R. Furfaro. "An Autonomous Sensor Tasking Approach for Large Scale Space Object Cataloging." In *Advanced Maui Optical and Space Surveillance Technologies Conference (AMOS)*, pages 1-17, 2017

[21] C. Frueh. "Sensor Tasking for Mulit-Sensor Object Surveillance." In *7th European Conference on Space Debris*, Darmstadt, Germany, Apr. 2017.

[22] A. D. Jaunzemis, M. J. Holzinger, and M. K. Jah. "Evidence-based Sensor Tasking for Space Domain Awareness." In *Advanced Maui Optical and Space Surveillance Technologies Conference*, Maui, HI, 2016. Maui Economic Development Board.

[23] Schildknecht, T., "Optical surveys for space debris", *The Astronomy and Astrophysics Review*, Vol. 14, No. 1, 2007, pp. 41-111. https://doi-org.ezproxy.lib.purdue.edu/10.1007/s00159-006-0003-9

[24] Linares R. and Furfaro R., "Dynamic Sensor Tasking For Space Situational Awareness via Reinforcement Learning." In *Advanced Maui Optical and Space Surveillance Technologies Conference 2017*, Maui, HI, 2017. Maui Economic Development Board.

[25] K. Hill, P. Sydney, K. Hamada, R. Cortez, K. Luu, M. Jah, P. Schumacher, M. Coulman, J. Houchard, and D. Naho'olewa, "Covariance-Based Network Tasking for Optical Sensors." In *Advances in the Astronautical Sciences*, 136(July):769-786, 2010

[26] Z. Sunberg, S. Chakravorty and R. S. Erwin, "Information Space Receding Horizon Control for Multisensor Tasking Problems," in IEEE Transactions on Cybernetics, vol. 46, no. 6, pp. 1325-1336, June 2016, doi: 10.1109/TCYB.2015.2445744.

[27] J. R. Shell, "Optimizing Orbital Debris Monitoring with Optical Telescopes", In *Advanced Maui Optical Space Surveillance Technologies Conference*, 2010.

[28] Africano, J., Schildknecht, T., Matney, M., Kervin, P., Stansbery, E., and Flury, W., "A Geosynchronous Orbit Search Strategy," Space Debris, Vol. 2, No. 4, 2000, pp. 357–369. doi:10.1023/B:SDEB.0000030025.04930.08

[29] Dararutana, K., "Comparison of Novel Heuristic and Integer Programming Schedulers for the USAF Space Surveillance Network", *Wright-Patterson Air Force Base: AFIT*, 2020.

[30] Dzamba, T., and Enright, J., "Ground Testing Strategies for Verifying the Slew Rate Tolerance of Star Trackers", MDPI Sensors, Vol. 14, No. 14, 2014. doi:10.3390/s140303939